A retrospective 4D-MRI based on 2D diaphragm profiles for lung cancer patients

Danny Lee PhD, Siyong Kim PhD, Jatinder Palta PhD, Benjamin Lewis MSc, Paul Keall PhD, Taeho Kim PhD

Keywords: 4D-MRI, lung cancer, MRI reconstruction, MRI-guided radiotherapy, retrospective reconstruction

Abstract

Introduction

4D-MRI, compared to 4D-CT, provides better soft-tissue contrast for target delineation. However, motion artefacts are often observed due to residual breathing variations. This study is to present a retrospective 4D-MRI reconstruction method based on 2D diaphragm profiles to improve the quality of 4D-MR images in the presence of significant breathing variations.

Methods

The proposed 4D-MRI reconstruction method utilized diaphragm profiles (2D cine images on a single sagittal plan at the peak diaphragm) in conjunction with 4D-MR scans (2D-cine images on multiple pre-determined coronal planes along the anterior-posterior direction over a volume of interest). The diaphragm profile images were exploited to sort the 4D-MR scans by matching respiratory amplitude of diaphragm on the 4D-MR scans to the diaphragm profiles. To evaluate reconstructed 4D-MR images (ten 3D-MR images), sagittal images on ten 3D-MR images under free breathing (FB) and respiratory guidance (GB) were compared with diaphragm profile images (reference) from 13 healthy volunteers.

Results

Forty-four 4D-MR scan datasets were successfully reconstructed without distinct respiratory-related motion artefacts even with the presence of breathing variation. The differences in diaphragm profiles between the reference and corresponding reconstructed images in the mean of root mean square were similar between FB (3.5 mm) and GB (3.0 mm), confirming that the 4D-MRI reconstruction method was effective even with significant breathing variation.

Conclusions

The diaphragm profiles were utilized to reconstruct 4D-MR images with spatial reliability and a fixed scan time under FB and GB. Our method can provide reliable 4D information of thoracic and abdominal regions for MRI-guided radiotherapy.

Introduction

Four-dimensional (4D) imaging[1] can provide information on respiratory-induced tumour motion, deformation and volume changes, required for the treatment planning of thoracic and abdominal cancers in external beam radiation treatment. In treatment planning, 4D-CT[2, 3] is also considered to measure tumour location and surrounding organs prior to the determination of an appropriate treatment method (i.e. real-time tumour tracking,[4, 5] respiratory-gating with breath-hold[6-8] or abdominal compressed shallow breathing).[9, 10] However, compared to magnetic resonance imaging (MRI), 4D-CT sometimes makes inaccurate tumour and organ delineation due to the lack of soft-tissue contrast.[11, 12] In addition, 4D-CT scans can be acquired only in axial orientation which is perpendicular to the direction of the most dominant breathing motion (i.e. superior–inferior direction), often causing sub-optimal imaging quality.[13]

Contrary to this, MRI allows image acquisition in any image orientation (i.e. axial, sagittal and coronal) and an optimal scan direction can be chosen as needed to potentially obtain more accurate measurement of tumour motion and range.[14] MRI also provides superior soft-tissue contrast required for precise tumour delineation in conventional radiotherapy and tumour tracking in MR-guided radiotherapy (i.e. hybrid MRI-radiotherapy).[15-19] Given the advantages of MRI over other imaging modalities including 4D imaging techniques, 4D-MRI is a valuable milestone for MR-guided radiotherapy.[20-22]

Two main approaches of 4D-MRI are retrospective sorting and prospective gating (or triggering). In the retrospective sorting approach, 2D images are acquired in a sequential mode (i.e. single acquisition in one slice and move to next slice to the end slice, then repeat) or a cine mode (i.e. acquisition over time in one slice then move to next to the end slice), and then sorted by a sorting method. There have been various sorting methods reported; the 2D images were sorted by respiratory amplitude (or phase) corresponding to different respiratory states of internal and external respiratory motion signals.[23, 24] Siebenthal et al.[25] obtained 4D-MR images by using a sorting method based on frame similarity of 2D images; Cai et al.[12] and Yang et al.[25] utilized image pixel values of 2D axial images; external respiratory bellows/internal MRI navigators were chosen in a study by Hui et al.[26]; Stemkens et al.[27, 28] used 3D deformation vector field information; and mutual information was utilized by Paganelli et al.[29] In prospective approaches, 3D images are obtained when triggered at multiple pre-determined respiratory amplitudes. There have been various triggering methods; Hu et al.[30] used a bellows belt; To et al.[31] used an air-filled cushion; Yang et al.[32] used an MR pulse sequence of 3D radial k-space sampling; and Han et al.[33] used an MR pulse sequence of 3D spiral k-space sampling.

Both retrospective and prospective approaches have been continuously improved, but there are still weaknesses. For instance, prospective imaging techniques[30, 32, 33] frequently require a long total scan time when breathing motion varies from breath to breath and the image quality can be highly subject to the size of the respiratory triggering window.[27, 30, 32-34] On the other hand, retrospective image techniques[29, 35, 36] often suffer from considerable image artefacts (i.e. streak, duplicate, blurring and incompletion) due to breathing variation.[13]

In this study, we introduced a retrospective 4D-MRI reconstruction method, utilizing multiple diaphragm profile images (2D cine images on a single sagittal plan acquired at the peak diaphragm). Ten diaphragm profiles (i.e. an upper boundary of diaphragm) corresponding to the ten reference respiratory states were utilized to sort and match diaphragm positions on 4D-MR scans (2D cine images on multiple pre-determined coronal planes along the anterior–posterior direction over a volume of interest) to each diaphragm profile, thereby improving the efficiency of retrospective 4D-MRI reconstruction with minimal respiratory-related sorting artefacts and without a long scan time.

Methods

Here, 4D-MR images are reconstructed by matching diaphragm amplitudes between diaphragm profiles and 4D-MR scans. The following sections describe (i) the process of the proposed method, (ii) MR image acquisitions and (iii) quantification.

4D-MR image reconstruction method based on diaphragm profiles

The method is comprised of three steps: (i) 2D diaphragm profile imaging, (ii) 4D-MR scans and (iii) retrospective reconstruction. The workflow of the method is illustrated in Figure 1 followed by a description of the study.

Step 1: 2D sagittal images at the peak diaphragm (i.e. where the diaphragm takes the superior-most location) were acquired over a few breathing cycles (see the square-dotted-box in 1.1 of Fig. 1). The superior boundary of the diaphragm (i.e. upper liver dome) in each sagittal image was identified by auto-segmentation using a region growing algorithm with a seed point previously described by Lee et al.,37 and then all of the images were sorted by the peak diaphragm position to determine ten sagittal images at ten respiratory amplitude bins equally spaced within a breathing cycle (i.e. 1 bin at inhalation peak, 4 bins in exhalation period, 1 bin at exhalation peak and 4 bins in inhalation period – see 1.2 of Fig. 1). Ten diaphragm profiles (blue-solid line) corresponding to the ten respiratory amplitude bins were used as reference diaphragm profiles in the later steps.

Step 2: 4D-MR scans (i.e. 2D cine image acquisition on multiple pre-determined coronal planes in this study – see the horizontal solid lines in 2.1 of Fig. 1) were acquired. The interval of coronal planes depended on the MRI slice thickness (i.e. 5 mm in this study). Here, 2D cine images were acquired over a few breathing cycles in each coronal plane. The diaphragm position (see the yellow dots in 2.2 of Fig. 1) was directly measured from each coronal image at the horizontal dotted line where is the intersection between sagittal and coronal imaging. Then, the 4D-MR scans were sorted according to the diaphragm position within each coronal plan and across all coronal planes. Yellow dotted lines indicate continuous diaphragm positions (diaphragm profile) along all coronal plans at each respiratory state.

Step 3: Retrospective image reconstruction was completed by matching respiratory amplitudes between their diaphragm profiles (see the yellow dotted line in 3.1 of Fig. 1) with that of corresponding reference diaphragm profiles (see the blue-solid-line in 3.1 of Fig. 1). Obviously, the 4D-MR image set consisted of ten 3D-MR image sets, one at each of the ten respiratory amplitude bins obtained in Step 1. For coronal planes where the diaphragm was invisible (e.g. chest and back),

variation in the sum of image intensity over the intersected line between the coronal and sagittal plane was utilized for binning.

MRI data acquisitions

Thirteen healthy volunteers participated in this study and each volunteer underwent two MRI sessions on different dates except for the first four volunteers (see Table 1). Each session included diaphragm profile imaging and 4D-MR scans with free breathing (FB). To investigate the effectiveness of the method under breathing variation, image acquisitions were made both with and without audiovisual breathing guidance.[38, 39] Obviously, more breathing variation in both phase and amplitude is expected without guidance than with. Hereafter, free breathing with guidance is noted as GB (Guided free Breathing) while free breathing without guidance just as FB. For 4D-MR scans, a fast 2D gradient-recalled-echo (fGRE) MR pulse sequence at a 3T GE MRI scanner (GE Healthcare) was used and its parameters were TR/TE = 2.64/1.17 ms, slice thickness = 5 mm, FOV = 480 × 384 mm^2, Flip angle = 20°, parallel imaging factor = 1 and pixel size = 1.875 × 1.875 mm^2. Diaphragm profile imaging on a sagittal plane (see Step 1 in Fig. 1) was performed for about 14 s (about 70 images = 14000 ms/196 ms) and 4D-MR scans (Step 2 in Fig. 1) for 296–400 s (up to 2016 images = 42 images/coronal plane × 48 coronal planes with 5 mm thickness along anterior–posterior [AP] direction). Table 1 shows the imaging characteristics (including the number of total images and acquisition time per each scan) of 4D-MR scans across 13 volunteers.

Abdominal respiratory motion signals were acquired using a real-time position management system (RPM: Varian Medical Systems, Palo Alto, USA) for audiovisual breathing guidance and also for a qualitative comparison of breathing regularity.[38, 39]

Image reconstruction and quantification

Forty-four 4D-MR scan datasets obtained from thirteen healthy volunteers were reconstructed based on the method described in section II.A. Prior to Steps 1.2 and 2.2 in Figure 1, MR images were saved in a Digital Imaging and Communications in Medicine (DICOM) format and the DICOM image datasets were proceeded in Matlab R2016B 64-bit (MathWorks, Natick, MA, USA).

Qualitative outcomes were compared using examples of reconstructed images with FB and GB, and quantitative outcomes in terms of diaphragm profiles were compared between reference diaphragm profiles and correspondent diaphragm profiles on 3D-MR images in a root mean square (RMS) and the P-value of a two-sided Wilcoxon signed rank test.[40]

Results

Image quality evaluation of reconstructed images

Figure 2 shows planar images from 4D-MR reconstruction at the full exhalation respiratory amplitude from the first volunteer, V01, together with the reference diaphragm profile images for both FB and GB cases. In addition, abdominal AP motion trajectory monitored with the RPM system is shown.

For the first volunteer, image quality of the reconstructed images under GB is better than that under FB (see arrows). Diaphragm position mismatch can be observed in certain areas of the sagittal image under FB. However, the method reconstructed 4D-MR images without significant image artefacts (i.e. no missing data points) for both FB (a large breathing variation) and GB (a small breathing variation) cases. Note that the coronal images and the reference sagittal images are directly obtained with finer resolution in the display plane (i.e. 1.875 mm × 1.875 mm) than that (i.e. 5 mm × 1.875 mm) of the reconstructed images (i.e. sagittal and axial images). Vertical streaks on the sagittal and axial images are also visible, which are due to the relatively larger imaging thickness (i.e. 5 mm).

Figure 3 shows planar images at ten respiratory amplitude bins from 4D-MR images with FB and GB (top-sagittal, mid-axial and bottom-coronal) from volunteer, V02.

For the second volunteer, the method with FB reconstructed 4D-MR images with some streak artefacts at inhalation (see the third and fourth images in Fig. 3a) due to breathing motion variability during acquisitions, but they are substantially reduced on 4D-MR images with GB (see Fig. 3b) due to improved breathing motion consistency.

Figure 4 shows the comparison of two reconstruction methods: a conventional phase-based sorting and the method in the breathing condition. The sagittal images were reconstructed in the breathing condition of V02 shown in Figure 3(a) for FB and (b) for GB. The method presents the significant improvement of image sorting and binning efficiency.

Image miss-alignment artefacts can be clearly found at the upper diaphragm region in the conventional phase-based sorting but it is almost eliminated in the method.

Figure 5 shows two sagittal images of a diaphragm profile image and a reconstructed sagittal image at the same respiratory amplitude bin for comparison of the diaphragm profiles for the volunteer V02.

The blue solid line and yellow-dotted line show the absolute position of diaphragm profile on a reference diaphragm profile image and a reconstructed sagittal image, respectively. There is a similar difference between the blue solid and yellow-dotted lines in both FB and GB.

Table 2 shows the RMS difference of two diaphragm profiles between reference diaphragm profile images and reconstructed sagittal images across ten respiratory amplitudes for every session from all of the volunteers. Mean values of RMS are also provided for both session-wise (last column) and bin-wise (bottom 2 rows) comparison. Note bin-wise mean values were obtained separately between FB and GB.

For thirteen volunteers, the method reconstructed 4D-MR images without missing data points for both FB and GB cases but GB improved the diaphragm profile difference by 0.5 mm (P-value < 0.001). The overall mean RMS values of the diaphragm profile difference across thirteen volunteers were 3.5 ± 1.1 mm and 3.0 ± 0.7 mm for FB and GB, respectively. RMS of diaphragm profile difference with GB was smaller in most sessions except for 6 of 22 sessions (V05-S2, V06-S2, V08-S1, V08-S2, V09-S1 and V13-S1) and it was larger at inhalation (i.e. bins 5 and 6) and exhalation (i.e. bins

1 and 10) in most sessions except for three sessions (V07-S2, V13-S1 and V13-S2). V06 had an irregular respiratory-induced diaphragm motion at the beginning of inhalation in the first FB and GB session which caused increased image miss alignment artefacts (~ 5.0 mm). However, it became regular in the second FB and GB session (~ 2.0 mm).

Discussion

In this study, we introduced a prospective 4D-MRI reconstruction based on diaphragm profiles. The method utilized reference diaphragm profile images determined at ten respiratory amplitude bins and 4D-MR scans along coronal planes. Diaphragm profile matching was performed across forty-four 4D-MR scan datasets, which successfully reconstructed 4D-MR images without substantial motion artefacts in the presence of irregular/regular breathing.

One of the limitations of 4D imaging is breathing variation from breathing cycle to cycle. To reduce the effect of the breathing variation in 4D-MRI, prospective imaging techniques[30, 32, 33] utilize a scan triggering method. However, prospective methods usually require a long total scan time and produce a low contrast resolution.[27, 30, 32-34] In contrast, conventional retrospective 4D-MRI methods[29, 35, 36] utilize a sorting method based on respiratory surrogate signals thus, requiring much shorter imaging time. But, breathing variation remains in the reconstruction process, often resulting in considerable image artefacts (i.e. streak, duplicate, blurring and incompletion).[13] The method, although it is a retrospective 4D-MRI method, reconstructs 4D-MR images using an image-driven amplitude-based binning approach instead of using an external surrogate approach thus, is expected to be less susceptible to intra-fractional breathing variation as demonstrated in this study (see Figs 2 and 3).

The method is free from external surrogates thus, expected to provide both setup flexibility and patient comfort, and can be applied to conventional MRI scanners without MR pulse sequence modification. In addition, the method could avoid an averaging of tumour motion at pre-determined respiratory triggering windows, required for a promising 4D-MRI reconstruction method and applicable for precise lung and abdominal tumour imaging.

This study has a few limitations. First, the 4D-MR images include vertical streaks on reconstructed sagittal and axial images due to relatively larger imaging thickness. We believe this issue can be resolved with effective image post-processing techniques of both image filtering[41] and window level adjusting, or by reducing the 2D-coronal slice thickness. Second, segmentation of the diaphragm required a relatively long time, with manual processing, to set an initial point for a region growing algorithm on 2D images.[37] With an automatic approach applied, we think, it can be improved in the future. Third, this method reconstructs 4D-MRI in a sequential order of ten bins from 1st bin to 10th bin, which could account for continuously increased image miss-alignment artefacts but it can be improved by analysing breathing motion regularity and applying during reconstruction. Last, we only evaluated the diaphragm position and shape accuracy of 4D-MR images from healthy subjects. Further studies with cancer patients are under consideration.

In conclusion, in this study, it was demonstrated that the retrospective 4D-MRI reconstruction based on diaphragm profiles without distinct image artefacts even with the presence of intra-fractional breathing variation. Our results suggest that 4D information of respiratory-induced motion in the thoracic and abdominal regions can be obtained using the method. The proposed method has potential applications for lung and abdominal cancer patients in MRI-guided treatment systems and integrated PET/MRI scanners.

Acknowledgements

This work has been partially supported by Institutional Research Grant IRG-14-192-40 from the American Cancer Society, United States and ECF181252 from Cancer Institute New South Wales, Australia.

References

1 Hugo, GD, Rosu, M. Advances in 4D radiation therapy for managing respiration: Part I–4D imaging. Zeitschrift für Medizinische Physik 2012; 22: 258– 71.

2 Keall, P, 4-dimensional computed tomography imaging and treatment planning. Sem Rad Oncol 2004; 14: 81– 90.

3 Rietzel, E, Liu, AK, Doppke, KP et al. Design of 4D treatment planning target volumes. Int J Rad Oncol* Biol* Physics 2006; 66: 287– 95.

4 Keall, PJ, Colvill, E, O'Brien, R et al. The first clinical implementation of electromagnetic transponder-guided MLC tracking. Med Phys 2014; 41: 020702.

5 Shah, AP, Kupelian, PA, Waghorn, BJ et al. Real-time tumor tracking in the lung using an electromagnetic tracking system. Int J Rad Oncol* Biol* Phys 2013; 86: 477– 83.

6 Wong, JW, Sharpe, MB, Jaffray, DA et al. The use of active breathing control (ABC) to reduce margin for breathing motion. Int J Rad Oncol* Biol* Phys 1999; 44: 911– 9.

7 Peng, Y, Vedam, S, Chang, JY et al. Implementation of feedback-guided voluntary breath-hold gating for cone beam CT-based stereotactic body radiotherapy. Int J Rad Oncol* Biol* Phys 2011; 80: 909– 17.

8 Park, Y-K, Kim, S, Kim, H, Kim, IH, Lee, K, Ye, S-J. Quasi-breath-hold technique using personalized audio-visual biofeedback for respiratory motion management in radiotherapy. Med Phys 2011; 38: 3114– 24.

9 Eccles, CL, Patel, R, Simeonov, AK, Lockwood, G, Haider, M, Dawson, LA. Comparison of liver tumor motion with and without abdominal compression using cine-magnetic resonance imaging. Int J Rad Oncol* Biol* Phys 2011; 79: 602– 8.

10 Wunderink, W, Romero, AM, De Kruijf, W, De Boer, H, Levendag, P, Heijmen, B. Reduction of respiratory liver tumor motion by abdominal compression in stereotactic body frame, analyzed by tracking fiducial markers implanted in liver. Int J Rad Oncol* Biol* Phys 2008; 71: 907– 15.

11 Akino, Y, Oh, RJ, Masai, N, Shiomi, H, Inoue, T. Evaluation of potential internal target volume of liver tumors using cine-MRI. Med Phys 2014; 41: 111704.

12 Yang, J, Cai, J, Wang, H et al. Four-dimensional magnetic resonance imaging using axial body area as respiratory surrogate: Initial patient results. Int J Rad Oncol* Biol* Phys 2014; 88: 907– 12.

13 Yamamoto, T, Langner, U, Loo, BW, Shen, J, Keall, PJ. Retrospective analysis of artifacts in four-dimensional CT images of 50 abdominal and thoracic radiotherapy patients. Int J Rad Oncol* Biol* Phys 2008; 72: 1250– 8.

14 Fernandes, AT, Apisarnthanarax, S, Yin, L et al. Comparative assessment of liver tumor motion using cine–magnetic resonance imaging versus 4-dimensional computed tomography. Int J Rad Oncol* Biol* Phys 2015; 91: 1034– 40.

15 Fallone, B, Murray, B, Rathee, S et al. First MR images obtained during megavoltage photon irradiation from a prototype integrated linac-MR system. Med Phys 2009; 36: 2084.

16 Kolling, S, Oborn, B, Keall, P. Impact of the MLC on the MRI field distortion of a prototype MRI-linac. Med Phys 2013; 40: 121705.

17 Lagendijk, JJ, Raaymakers, BW, Raaijmakers, AJ et al. MRI/linac integration. Radiother Oncol 2008; 86: 25– 9.

18 Raaymakers, B, Lagendijk, J, Overweg, J et al. Integrating a 1.5 T MRI scanner with a 6 MV accelerator: proof of concept. Phys Med Biol 2009; 54: N229.

19 Mutic, S, Dempsey, JF. The ViewRay system: Magnetic resonance–guided and controlled radiotherapy. Sem Rad Oncol 2014; 24: 196– 9.

20 Keall, PJ, Barton, M, Crozier, S. The Australian magnetic resonance imaging–linac program. Sem Rad Oncol 2014; 24: 203– 6.

21 Lagendijk, JJ, Raaymakers, BW, Vulpen, M. The magnetic resonance imaging–linac system. Sem Rad Oncol 2014; 24: 207– 9.

22 Fallone, BG. The rotating biplanar linac–magnetic resonance imaging system. Sem Rad Oncol 2014; 24: 200– 2.

23 Fitzpatrick, MJ, Starkschall, G, Antolak, JA et al. Displacement-based binning of time-dependent computed tomography image data sets. Med Phys 2006; 33: 235– 46.

24 Abdelnour, A, Nehmeh, S, Pan, T et al. Phase and amplitude binning for 4D-CT imaging. Physics Med Biol 2007; 52: 3515.

25 Siebenthal, M, Gamper, U, Boesiger, P, Lomax, A, Cattin, P. 4D MR imaging of respiratory organ motion and its variability. Phys Med Biol 2007; 52: 1547.

26 Hui, C, Wen, Z, Stemkens, B et al. 4D MR imaging using robust internal respiratory signal. Phys Med Biol 2016; 61: 3472.

27 Stemkens, B, Tijssen, RH, Senneville, BD et al. Optimizing 4-dimensional magnetic resonance imaging data sampling for respiratory motion analysis of pancreatic tumors. Int J Radiat Oncol Biol Phys 2015; 91: 571– 8.

28 Stemkens, B, Tijssen, RH, Senneville, BD, Lagendijk, JJ, Berg, CA. Image-driven, model-based 3D abdominal motion estimation for MR-guided radiotherapy. Phys Med Biol 2016; 61: 5335.

29 Paganelli, C, Summers, P, Bellomi, M, Baroni, G, Riboldi, M. Liver 4DMRI: a retrospective image-based sorting method. Med Phys 2015; 42: 4814– 21.

30 Hu, Y, Caruthers, SD, Low, DA, Parikh, PJ, Mutic, S. Respiratory amplitude guided 4-dimensional magnetic resonance imaging. Int J Rad Oncol* Biol* Phys 2013; 86: 198– 204.

31 To, DT, Kim, JP, Price, RG, Chetty, IJ, Glide-Hurst, CK. Impact of incorporating visual biofeedback in 4D MRI. J Appl Clin Med Phys 2016; 17: 128– 37.

32 Yang, W, Fan, Z, Tuli, R et al. Four-dimensional magnetic resonance imaging with 3-dimensional radial sampling and self-gating–based K-space sorting: early clinical experience on pancreatic cancer patients. Int J Rad Oncol* Biol* Phys. 2015; 93: 1136– 43.

33 Han, F, Zhou, Z, Cao, M, Yang, Y, Sheng, K, Hu, P. Respiratory motion resolved, self-gated 4D-MRI using Rotating Cartesian K-space (ROCK). Med Phys 2017; 44: 1359– 68.

34 Lee, D, Greer, P, Arm, J, Keall, P, Kim, T. Audiovisual biofeedback improves image quality and reduces scan time for respiratory-gated 3D MRI. J Phys Conference Series: IOP Publishing 2014; 489: 012033.

35 Cai, J, Chang, Z, Wang, Z, Segars, WP, Yin, F-F. Four-dimensional magnetic resonance imaging (4D-MRI) using image-based respiratory surrogate: a feasibility study. Med Phys 2011; 38: 6384– 94.

36 Liu, Y, Yin, F-F, Rhee, D, Cai, J. Accuracy of respiratory motion measurement of 4D-MRI: a comparison between cine and sequential acquisition. Med Phys 2016; 43: 179– 87.

37 Lee, D, Greer, PB, Ludbrook, J et al. Audiovisual biofeedback improves cine-MRI measured lung tumor motion consistency. Int J Radiat Oncol Biol Phys 2015; 94: 628– 36.

38 Kim, T, Pollock, S, Lee, D, O'Brien, R, Keall, P. Audiovisual biofeedback improves diaphragm motion reproducibility in MRI. Med Phys 2012; 39: 6921– 8.

39 Lee, D, Greer, PB, Ludbrook, J et al. Audiovisual biofeedback improves cine–magnetic resonance imaging measured lung tumor motion consistency. Int J Rad Oncol* Biol* Phys 2016; 94: 628– 36.

40 Gibbons, JD, Chakraborti, S. Nonparametric statistical inference. Springer, Berlin, Heidelberg, 2011; 977– 9.

41 Behrenbruch, C, Petroudi, S, Bond, S, Declerck, J, Leong, F, Brady, J. Image filtering techniques for medical image post-processing: an overview. Brit J Radiol 2014; 77: 126– 32.

Figure Legends

Figure 1. The workflow of the method. Step 1. Diaphragm profile imaging – (Step 1.1) Using cine imaging on a sagittal plane (square-dotted-box) at the peak diaphragm, (Step 1.2) ten respiratory amplitude bins (equal space in millimeters) are obtained by the peak diaphragm position through the autosegmentation of the upper diaphragm (blue solid line). Step 2. 4D-MR scans – (Step 2.1) Using multiple cine imaging on coronal planes over a volume of interest (horizontal dotted line) along anterior–posterior direction, (Step 2.2) diaphragm position (each yellow-dot) is detected at the orthogonal position of the blue line and it is used to sort 4D-MR scans within each coronal plane and across also coronal plans. Yellow dotted lines indicate continuous diaphragm positions (diaphragm profile) along all coronal plans at each respiratory state. Step 3. Retrospective reconstruction – (Step 3.1) Complete 4D-MR images, the diaphragm profile (blue-solid-line) of each respiratory amplitude bin is compared with corresponding the diaphragm positions (yellow-dots) for 3D-MR images at the pre-determined ten respiratory amplitude bins).

Figure 2. A diaphragm profile image (reference) and 3 planar images from 4D-MR reconstruction at the full exhalation under (a) FB without guidance and (b) GB (FB with guidance) from the first volunteer (V01). Arrows highlight reduced respiration-induced-motion artefacts with GB compared with FB case. Vertical and horizontal dotted lines on coronal images indicate the sagittal and axial imaging planes. A: Anterior, P: Posterior, R: Right, L: Left, S: Superior and I: Inferior.

Figure 3. Planar images from 4D-MR reconstruction at all of 10 respiratory amplitude bins under (a) FB and (b) GB from the second volunteer (V02). The horizontal-solid-lines indicate the diaphragm position at the end of inhalation for easier comparison among different breathing amplitudes. Vertical and horizontal dotted lines on the first coronal images indicate the intersection of sagittal and axial images.

Figure 4. Reconstructed sagittal images using a conventional phase-based sorting (left column) and the method (right column) with FB and GB from V02 at the full inhalation.

Figure 5. A diaphragm profile image and a sagittal image of 3D-MR images with (a) FB and (b) GB in respect to the same diaphragm profiles. Sagittal images represent the image quality of 4D-MR images where was measured at 50 percentile of all 4D-MR image datasets.

Table 1. Imaging characteristics of 4D-MR scans in FB and GB

Volunteer subjects	Session no.	AP range (cm)	No. of images	Acquisition time (s)
V01	S1	24	1976	387
V02	S1	18	1512	296
V03	S1	24	1976	387
V04	S1	18	1512	296
V05	S1	24	2016	395
	S2	24	2016	395
V06	S1	24	1976	387
	S2	24	2016	395
V07	S1	24	2016	395
	S2	24	2016	395
V08	S1	24	2040	400
	S2	24	2040	400

Volunteer subjects	Session no.	AP range (cm)	No. of images	Acquisition time (s)
V09	S1	24	2016	395
	S2	24	2016	395
V10	S1	24	2016	395
	S2	24	2016	395
V11	S1	24	2016	395
	S2	24	2016	395
V12	S1	24	2016	395
	S2	24	2016	395
V13	S1	18	1482	290
	S2	18	1482	290

AP, anterior-posterior; FB, free breathing without guidance; GB, guided free breathing; S, session; V, volunteer.

Table 2. The difference of diaphragm profiles between reference diaphragm profiles and reconstructed sagittal images of 3D-MR images across ten respiratory amplitudes

Subjects	Sessions		Diaphragm profile difference at respiratory bins in RMS (mm)										
			Bin 1	Bin 2	Bin 3	Bin 4	Bin 5	Bin 6	Bin 7	Bin 8	Bin 9	Bin 10	Mean (±STD)
V01	S1	FB	1.9	2.3	3.0	3.7	6.7	6.3	3.3	2.9	1.9	1.7	3.4 ± 1.8
		GB	1.9	1.8	2.2	4.5	5.0	4.8	4.5	2.3	1.8	1.9	3.1 ± 1.4
V02	S1	FB	2.3	2.9	2.7	2.2	2.8	2.9	4.4	3.9	3.3	2.2	3.0 ± 0.7
		GB	3.6	2.4	2.1	3.2	2.4	2.4	3.4	2.2	2.6	4.0	2.8 ± 0.7
V03	S1	FB	5.0	5.6	5.3	5.5	5.7	5.3	6.0	5.6	5.9	6.4	5.6 ± 0.4

Subjects	Sessions		Diaphragm profile difference at respiratory bins in RMS (mm)									
			Bin 1	Bin 2	Bin 3	Bin 4	Bin 5	Bin 6	Bin 7	Bin 8	Bin 9	Bin 10	Mean (±STD)
		GB	1.5	1.6	1.8	2.3	3.4	3.4	2.3	2.0	1.6	1.5	2.1 ± 0.7
V04	S1	FB	4.8	3.8	3.4	4.1	3.5	3.4	4.1	3.5	4.0	5.0	4.0 ± 0.6
		GB	4.1	3.3	3.6	3.9	4.1	3.6	3.4	3.2	2.8	3.6	3.6 ± 0.4
V05	S1	FB	2.0	1.8	2.6	3.1	3.9	3.2	3.5	3.1	3.2	3.7	3.0 ± 0.7
		GB	2.3	2.3	2.9	3.3	3.2	3.3	3.5	2.5	2.3	2.0	2.8 ± 0.5
	S2	FB	2.7	1.9	2.2	1.6	1.8	1.8	1.7	2.0	1.7	1.7	1.9 ± 0.3

Subjects	Sessions		Diaphragm profile difference at respiratory bins in RMS (mm)									
			Bin 1	**Bin 2**	**Bin 3**	**Bin 4**	**Bin 5**	**Bin 6**	**Bin 7**	**Bin 8**	**Bin 9**	**Bin 10**	**Mean (±STD)**
		GB	5.1	4.0	2.2	3.2	3.7	2.8	3.2	2.0	3.7	5.1	3.5 ± 1.1
V06	S1	FB	6.2	6.4	5.4	4.2	3.5	3.3	3.9	5.1	5.2	6.3	5.0 ± 1.2
		GB	2.1	2.8	4.5	5.0	5.7	6.5	4.8	4.4	2.9	2.1	4.1 ± 1.5
	S2	FB	1.5	1.5	1.9	1.6	1.7	1.8	1.2	1.5	1.1	1.0	1.5 ± 0.3
		GB	2.8	2.1	1.4	1.4	2.2	2.2	1.3	1.2	1.9	3.5	2.0 ± 0.7
V07	S1	FB	3.4	2.7	3.2	1.8	4.0	4.1	1.8	3.0	2.6	3.0	3.0 ± 0.8

Subjects	Sessions		Diaphragm profile difference at respiratory bins in RMS (mm)									
			Bin 1	Bin 2	Bin 3	Bin 4	Bin 5	Bin 6	Bin 7	Bin 8	Bin 9	Bin 10	Mean (±STD)
		GB	2.7	2.7	2.5	3.1	2.6	2.6	3.2	2.3	2.7	2.6	2.7 ± 0.3
	S2	FB	4.3	3.2	6.3	3.3	4.0	3.1	3.2	6.1	3.0	4.1	4.1 ± 1.2
		GB	3.6	8.6	2.4	2.4	2.5	2.4	2.4	2.4	8.8	3.6	3.9 ± 2.6
V08	S1	FB	2.1	2.2	3.0	3.1	3.6	2.7	3.1	3.0	2.1	2.1	2.7 ± 0.5
		GB	2.1	2.2	3.2	2.8	4.0	4.4	2.8	3.1	2.1	2.0	2.9 ± 0.8
	S2	FB	3.2	2.8	3.0	2.9	3.0	2.8	2.9	3.1	2.9	3.4	3.0 ± 0.2

Subjects	Sessions		Diaphragm profile difference at respiratory bins in RMS (mm)									
			Bin 1	Bin 2	Bin 3	Bin 4	Bin 5	Bin 6	Bin 7	Bin 8	Bin 9	Bin 10	Mean (±STD)
		GB	3.6	3.4	3.5	3.2	3.6	3.4	3.2	3.5	3.4	3.6	3.4 ± 0.2
V09	S1	FB	2.2	2.1	2.1	2.3	2.5	4.9	2.7	2.3	2.1	5.3	2.9 ± 1.2
		GB	3.1	2.8	3.6	4.7	6.6	6.0	4.6	3.6	2.7	3.2	4.1 ± 1.4
	S2	FB	1.8	1.9	3.3	3.5	4.8	4.9	3.4	3.4	2.0	1.8	3.1 ± 1.2
		GB	1.8	2.0	1.9	1.8	2.2	2.3	2.2	1.8	1.8	2.3	2.0 ± 0.2
V10	S1	FB	2.1	1.8	1.9	2.7	4.6	4.3	2.3	1.6	2.0	1.3	2.5 ± 1.1

Subjects	Sessions		Diaphragm profile difference at respiratory bins in RMS (mm)									
			Bin 1	Bin 2	Bin 3	Bin 4	Bin 5	Bin 6	Bin 7	Bin 8	Bin 9	Bin 10	Mean (±STD)
V11	S1	GB	2.2	1.6	1.2	1.3	1.4	1.4	1.3	1.2	1.6	2.5	1.6 ± 0.4
		FB	2.0	2.0	2.6	3.2	4.1	5.8	4.4	3.5	2.6	5.2	3.5 ± 1.3
	S2	GB	2.6	2.0	1.9	1.9	2.6	2.6	1.9	1.9	1.9	2.3	2.2 ± 0.3
		FB	7.0	5.6	3.2	3.0	3.6	3.6	3.0	3.3	5.8	7.0	4.5 ± 1.7
	S1	GB	2.7	2.4	3.3	3.1	2.6	2.6	3.1	3.2	2.5	2.8	2.8 ± 0.3
		FB	4.7	4.4	4.2	3.7	3.7	3.7	3.7	4.2	4.4	4.8	4.2 ± 0.4
	S2												

Subjects	Sessions		Diaphragm profile difference at respiratory bins in RMS (mm)									
			Bin 1	Bin 2	Bin 3	Bin 4	Bin 5	Bin 6	Bin 7	Bin 8	Bin 9	Bin 10	Mean (±STD)
		GB	6.5	4.3	2.4	2.2	2.5	2.6	2.0	2.3	4.8	6.2	3.6 ± 1.7
V12	S1	FB	7.7	7.4	7.0	6.4	6.2	3.0	2.8	2.9	6.9	5.8	5.6 ± 2.0
		GB	2.9	2.2	2.3	2.7	3.2	3.1	2.9	2.5	2.3	2.8	2.7 ± 0.4
	S2	FB	3.9	4.0	3.8	4.5	5.2	5.3	4.5	3.8	4.0	3.9	4.3 ± 0.6
		GB	3.8	2.9	2.9	3.5	3.7	3.7	3.7	2.9	2.9	3.9	3.4 ± 0.4
V13	S1	FB	1.7	3.5	3.2	4.1	2.9	2.9	4.7	3.2	3.5	2.7	3.2 ± 0.8

Subjects	Sessions		Diaphragm profile difference at respiratory bins in RMS (mm)									
			Bin 1	**Bin 2**	**Bin 3**	**Bin 4**	**Bin 5**	**Bin 6**	**Bin 7**	**Bin 8**	**Bin 9**	**Bin 10**	**Mean (±STD)**
		GB	4.3	4.6	3.7	3.5	2.1	2.1	3.5	3.8	4.7	4.3	3.7 ± 0.9
	S2	FB	4.1	4.4	3.9	3.8	3.0	2.9	3.9	3.8	4.3	4.0	3.8 ± 0.5
		GB	2.8	2.7	1.9	2.0	1.9	1.9	1.9	1.8	2.6	2.9	2.2 ± 0.4
Mean (STD)		FB	3.5 ± 1.8	3.4 ± 1.7	3.5 ± 1.4	3.4 ± 1.2	3.9 ± 1.3	3.7 ± 1.2	3.4 ± 1.1	3.4 ± 1.1	3.4 ± 1.5	3.7 ± 1.8	3.5 ± 1.1
		GB	3.1 ± 1.2	2.9 ± 1.5	2.6 ± 0.8	3.0 ± 1.0	3.2 ± 1.3	3.2 ± 1.3	3.0 ± 1.0	2.6 ± 0.8	2.9 ± 1.6	3.1 ± 1.1	3.0 ± 0.7

Figure 1

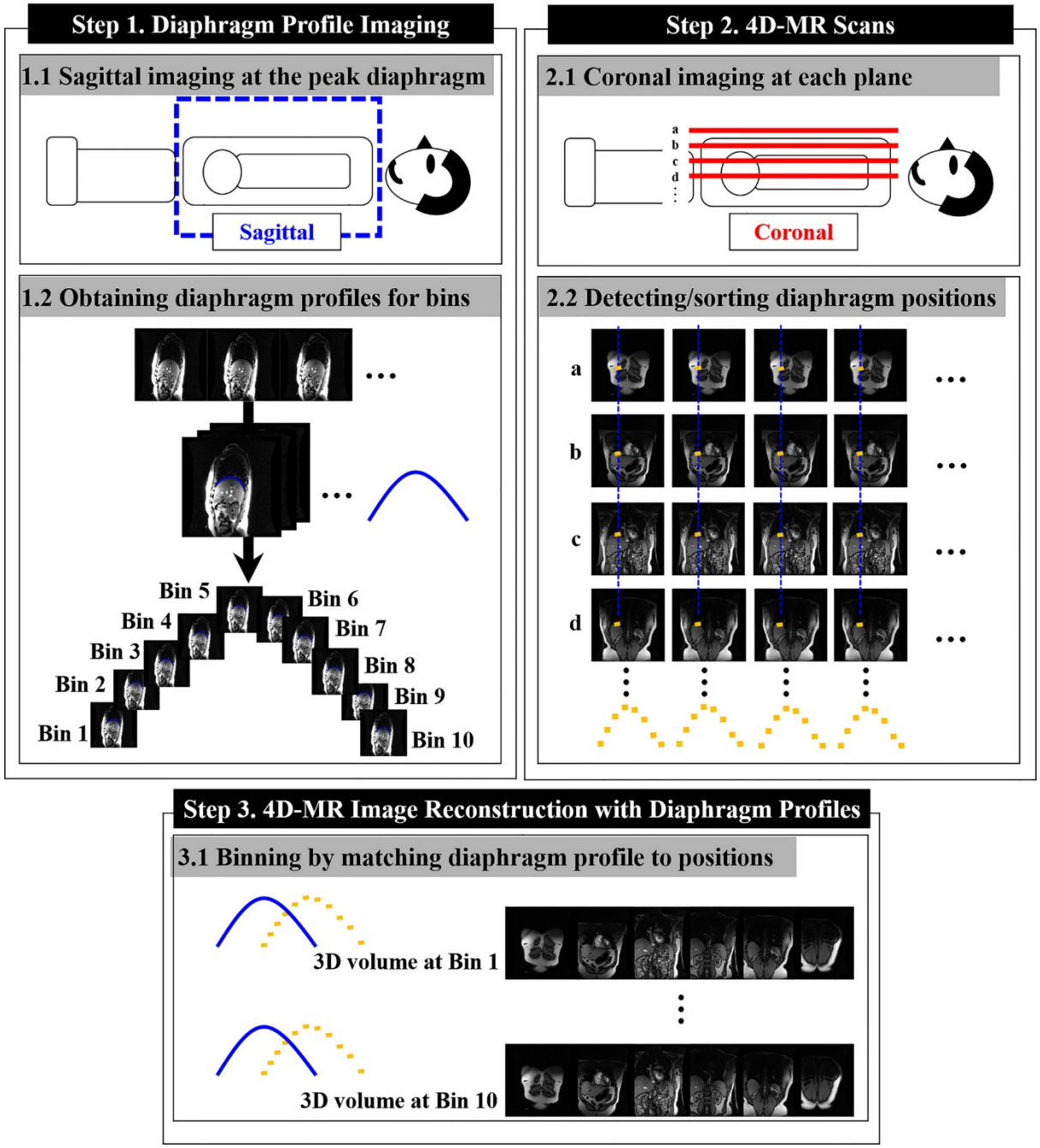
Step 1. Diaphragm Profile Imaging
1.1 Sagittal imaging at the peak diaphragm
Sagittal
1.2 Obtaining diaphragm profiles for bins
Bin 1
Bin 2
Bin 3
Bin 4
Bin 5
Bin 6
Bin 7
Bin 8
Bin 9
Bin 10
Step 2. 4D-MR Scans
2.1 Coronal imaging at each plane
a
b
c
d
Coronal
2.2 Detecting/sorting diaphragm positions
a
b
c
d
Step 3. 4D-MR Image Reconstruction with Diaphragm Profiles
3.1 Binning by matching diaphragm profile to positions
3D volume at Bin 1
3D volume at Bin 10

Figure 2.

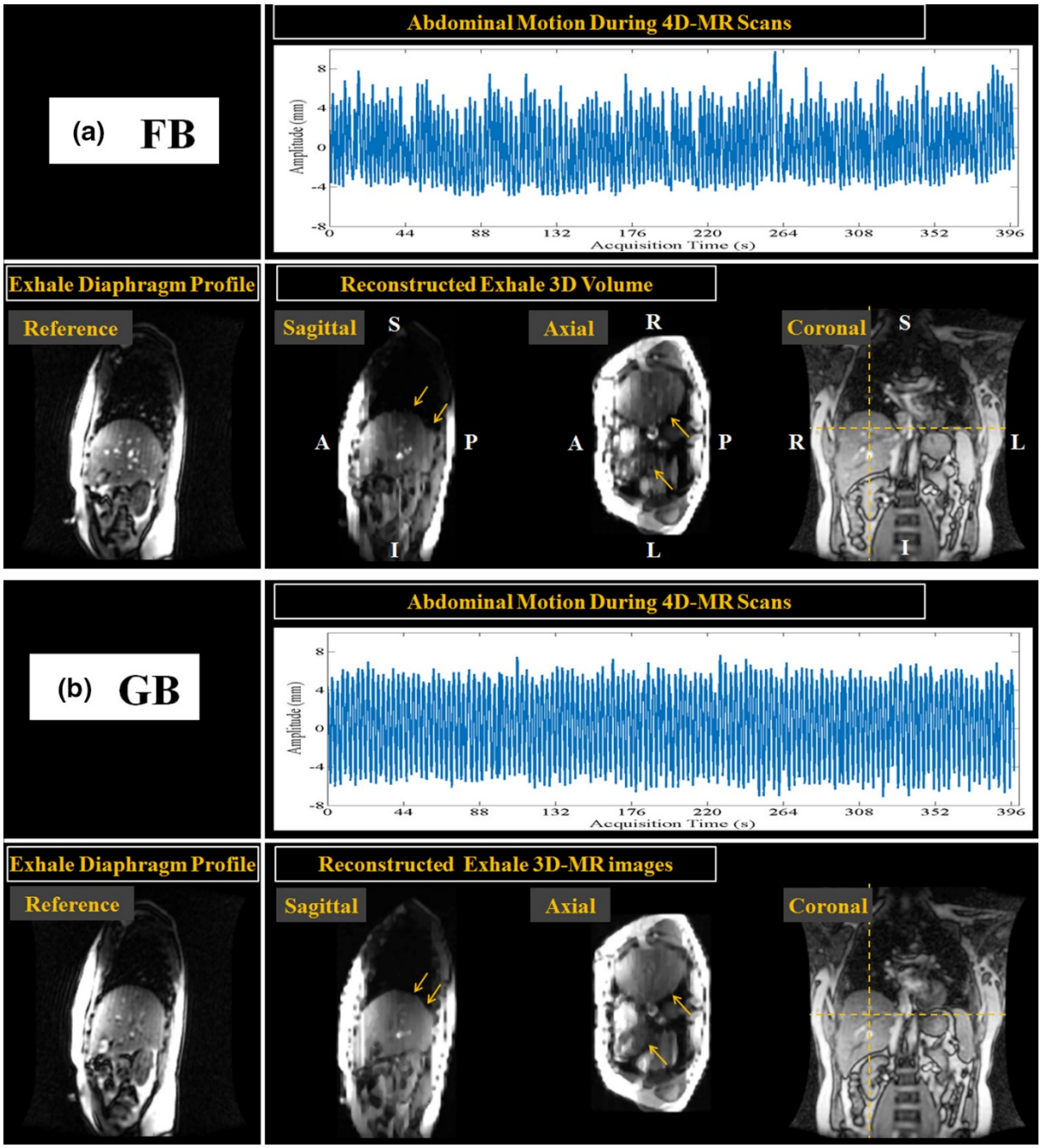
(a) FB
Abdominal Motion During 4D-MR Scans
Amplitude (mm)
Acquisition Time (s)
Exhale Diaphragm Profile
Reference
Reconstructed Exhale 3D Volume
Sagittal
Axial
Coronal
S
A
P
I
R
L
(b) GB
Abdominal Motion During 4D-MR Scans
Amplitude (mm)
Acquisition Time (s)
Exhale Diaphragm Profile
Reference
Reconstructed Exhale 3D-MR images
Sagittal
Axial
Coronal

Figure 3.

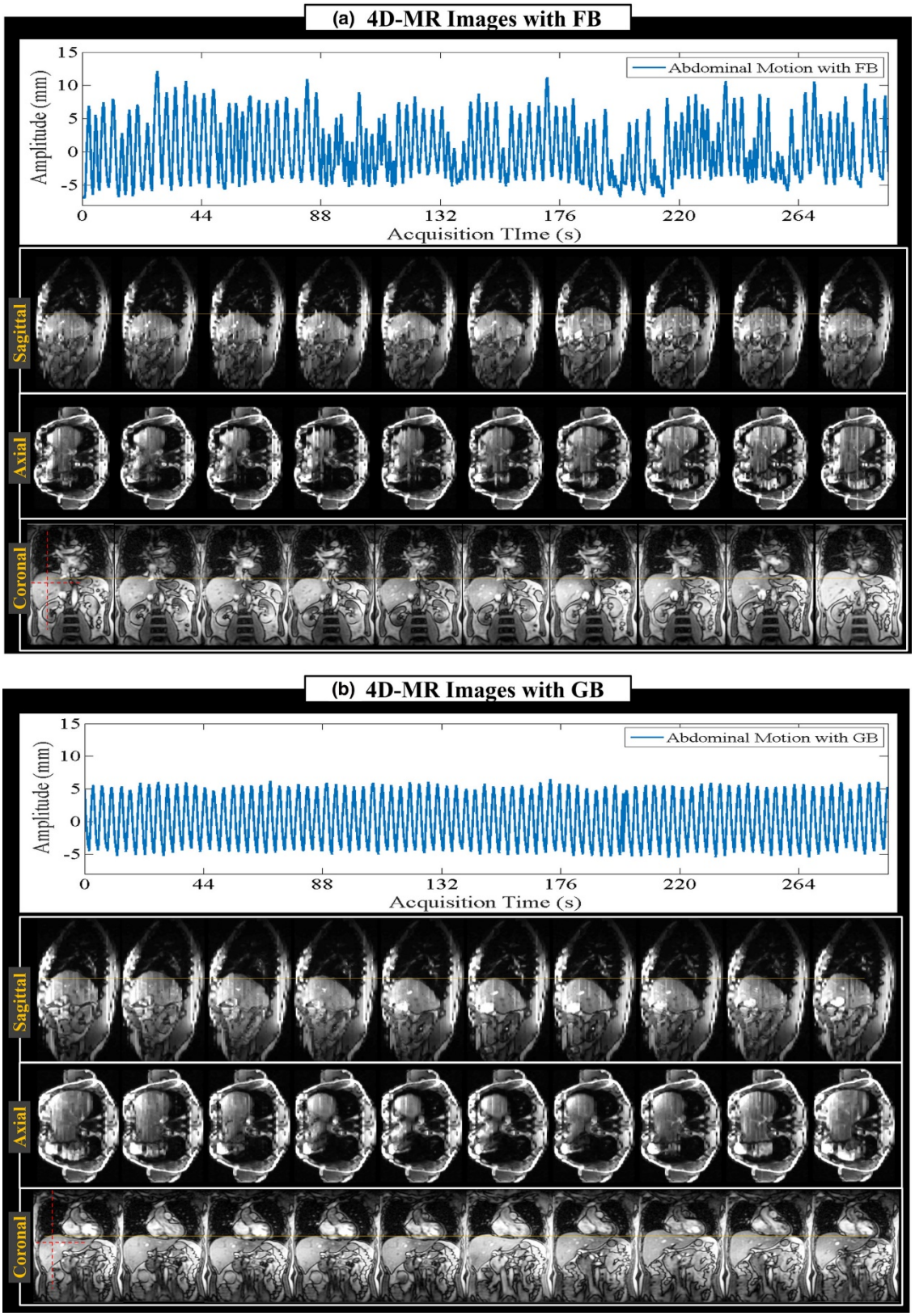
(a) 4D-MR Images with FB
Abdominal Motion with FB
Amplitude (mm)
15
10
5
0
-5
0
44
88
132
176
220
264
Acquisition TIme (s)
Sagittal
Axial
Coronal
(b) 4D-MR Images with GB
Abdominal Motion with GB
Amplitude (mm)
15
10
5
0
-5
0
44
88
132
176
220
264
Acquisition Time (s)
Sagittal
Axial
Coronal

Figure 4.

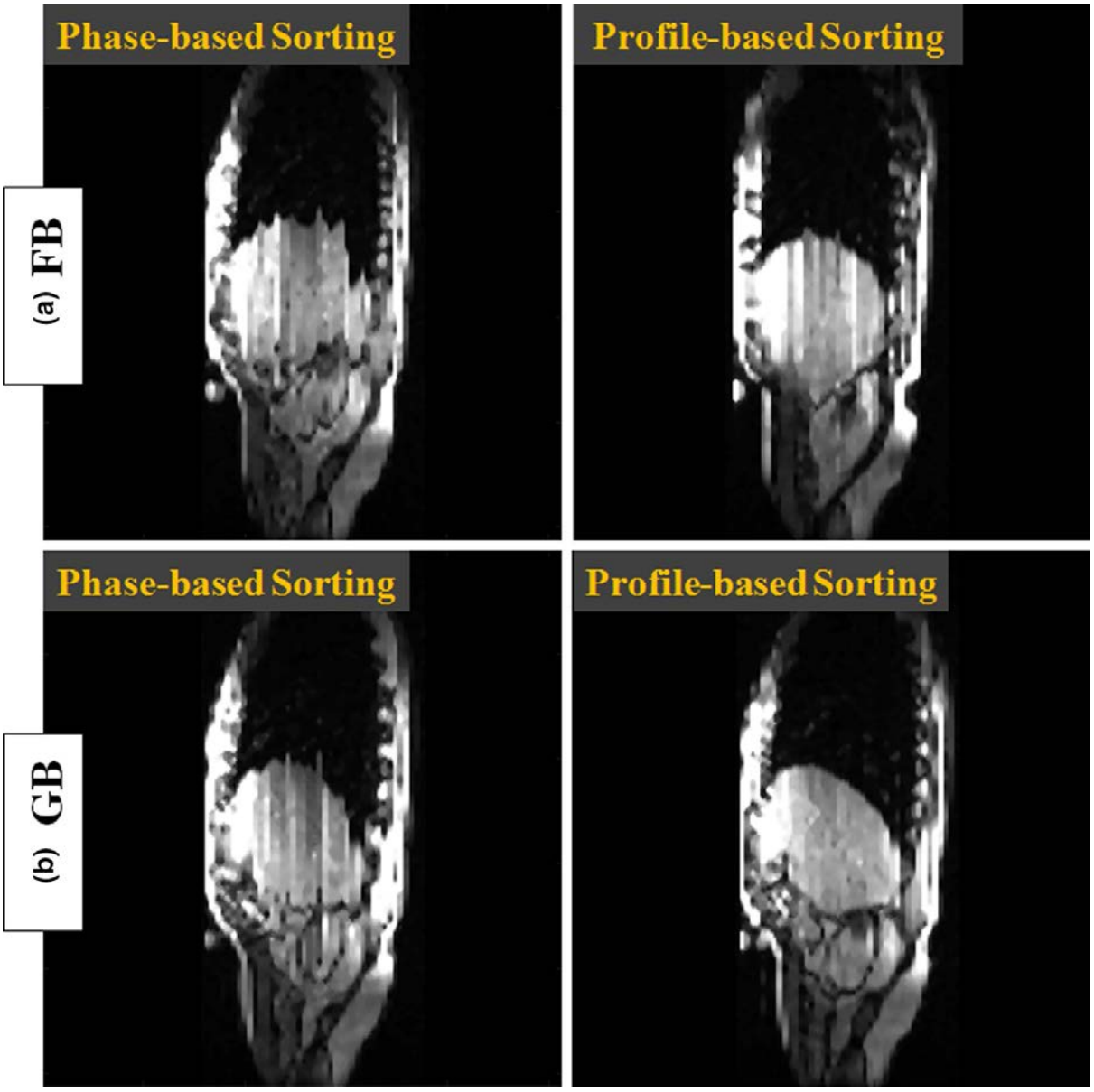
Phase-based Sorting
Profile-based Sorting
(a) FB
Phase-based Sorting
Profile-based Sorting
(b) GB

Figure 5.

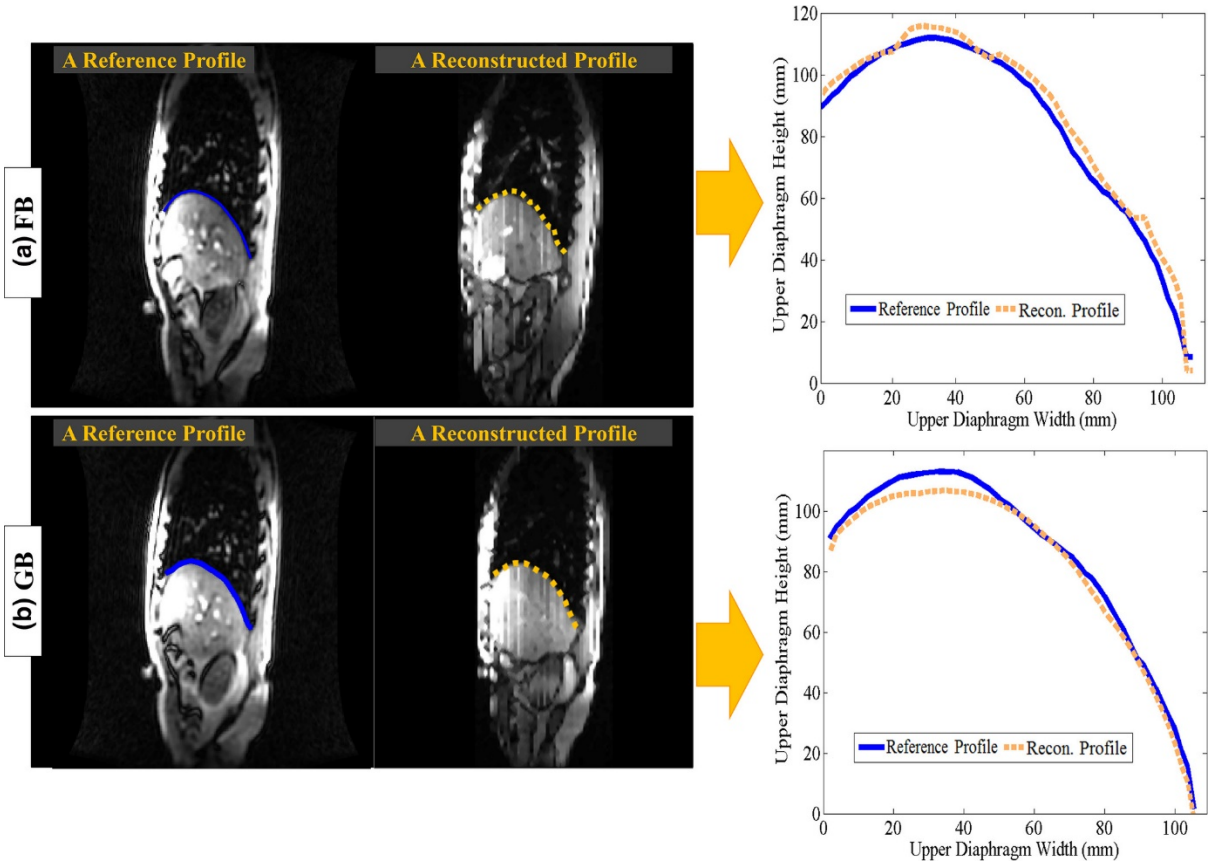
A Reference Profile
A Reconstructed Profile
(a) FB
A Reference Profile
A Reconstructed Profile
(b) GB
Upper Diaphragm Height (mm)
Upper Diaphragm Width (mm)
Reference Profile
Recon. Profile
Upper Diaphragm Height (mm)
Upper Diaphragm Width (mm)
Reference Profile
Recon. Profile